

## Supporting Information

### Mesoporous TiO<sub>2</sub> Single Crystals: Facile Shape-, Size- and Phase-controlled Growth and Efficient Photocatalytic Performance

Xiaoli Zheng, Qin Kuang, Keyou Yan, Yongcai Qiu, Jianhang Qiu, and Shihe Yang\*

Department of Chemistry, The Hong Kong University of Science and Technology, Clear Water Bay, Kowloon, Hong Kong

\*Corresponding Author. E-mail: chsyang@ust.hk

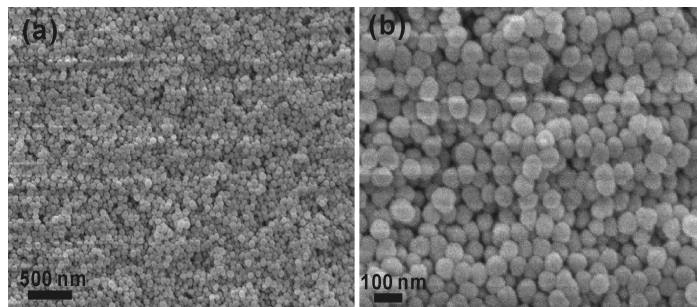


**Figure S1.** Low- (a) and large- (b) magnification SEM images of pristine silica template made up of quasi-close-packed silica beads (~50 nm in diameter).

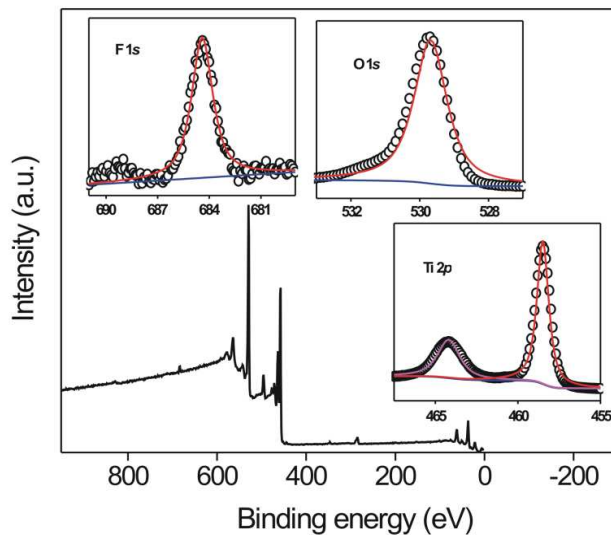


**Figure S2.** XPS spectra of anatase mesoporous nanosheets, showing the four characteristic peaks of Ti, O, F and C. The insets show the three characteristic peaks of Ti, O and F. The open circles are the raw data, and the blue and red/purple lines represent the base line and fitted lines, respectively.

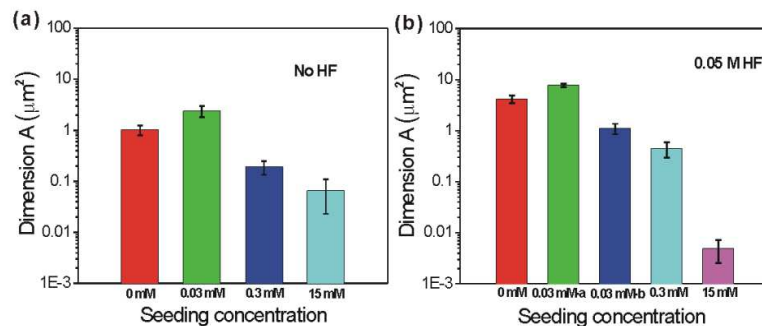


**Figure S3.** The size evolution of non-porous and mesoporous TiO<sub>2</sub> single crystals prepared at different conditions: (a) no HF and (b) 0.05 M HF, as a function of seeding concentration. 0.03 mM-a and 0.03 mM-b in (b) are represent of olive-shaped mesoporous TiO<sub>2</sub> and mesoporous nanosheets, respectively. Error bars represent the standard deviation of the measured sample distribution (minimum 50 samples).

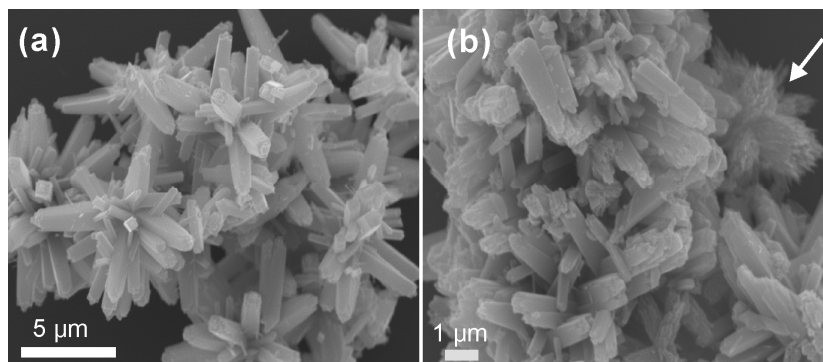


**Figure S4.** (a, b) SEM images of TiO<sub>2</sub> crystals prepared in the presence of non-seeded silica template, only very little mesoporous crystals that growing inside the silica template was observed (marked by the white arrow in (b)). Hydrothermal reaction condition is: 180°C, 12 h, 0.4 ml titanium butoxide.

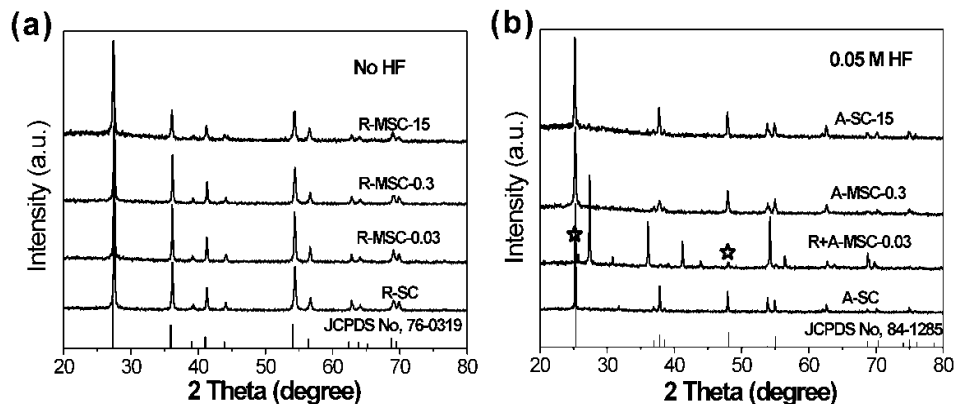


**Figure S5.** XRD patterns of (a) solid and TiO<sub>2</sub> MSCs obtained at different seeding concentrations, and (b) solid and TiO<sub>2</sub> MSCs obtained after addition of 0.05 M HF.

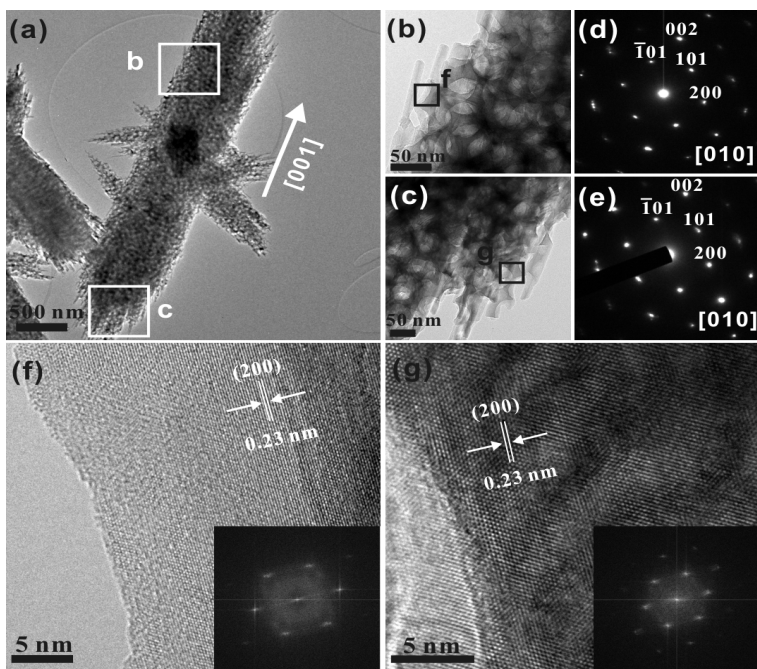


**Figure S6.** (a) TEM image of a single mesoporous TiO<sub>2</sub> branched-nanorod (seeding concentration: 0.03 mM, 180°C). (b,c) Enlarged TEM images and (d,e) corresponding SAED patterns of the areas labeled in (a). (f, g) HRTEM images and corresponding fast Fourier transform patterns (inset) of the areas labeled in (b) and (c), respectively. The coherent lattice fringes and the fast Fourier transform patterns further confirm its rutile single crystalline feature.

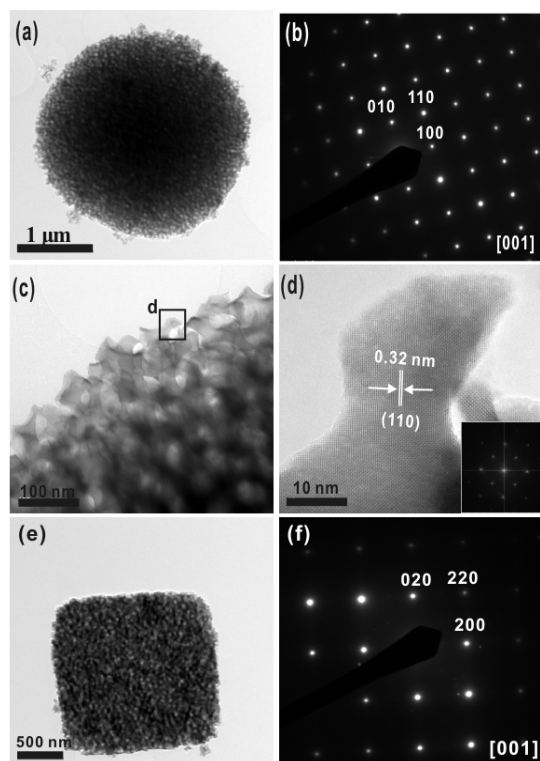


**Figure S7.** (a, b) TEM image and corresponding SAED pattern of a single olive-shaped rutile TiO<sub>2</sub> MSC (R-MSC-0.03, seeding concentration: 0.03 mM, HF: 0.05 M, 180°C). (c) Enlarged TEM image and (d) HRTEM image and corresponding fast Fourier transform patterns (inset) of the area labeled in (c). (e, f) TEM image and corresponding SAED pattern of a single anatase mesoporous TiO<sub>2</sub> nanosheet (A-MSC-0.03, seeding concentration: 0.03 mM, HF: 0.05 M, 180°C).

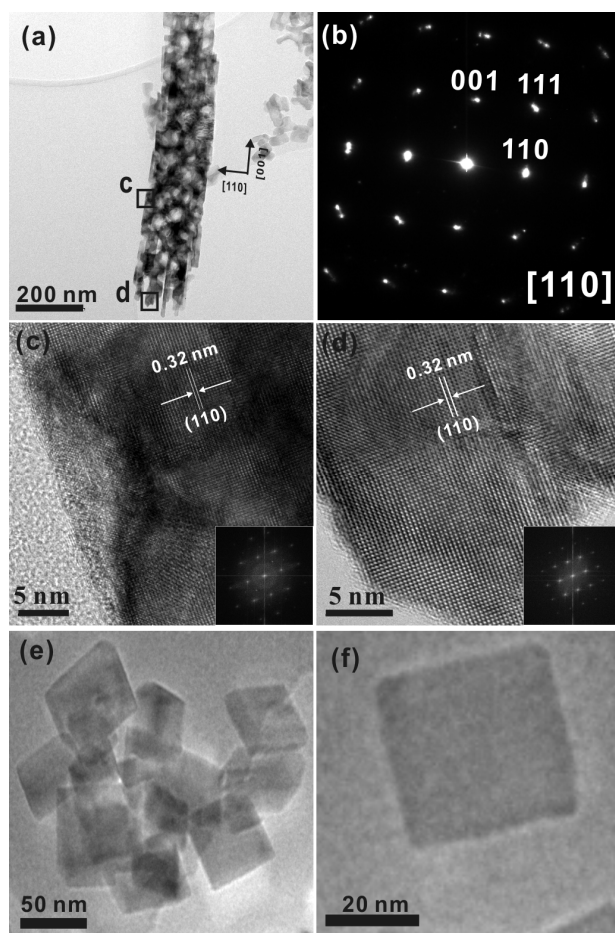


**Figure S8.** (a, b) TEM image and corresponding SAED pattern of a single thin-nanorod-shaped rutile TiO<sub>2</sub> MSC (R-MSC-15, seeding concentration: 15 mM, 180°C). (c, d) HRTEM images and corresponding fast Fourier transform patterns (inset) of the areas labeled in (a). (e, f) TEM images of non-porous anatase TiO<sub>2</sub> nanosheets (A-SC-15, seeding concentration: 15 mM, HF: 0.05 M, 180°C).

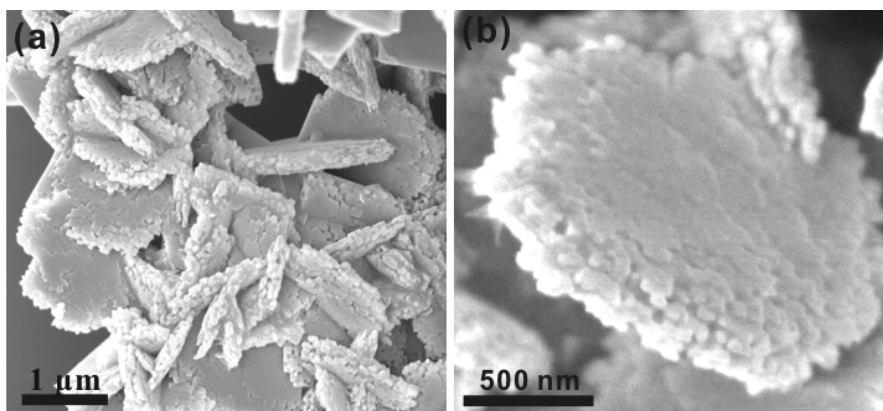


**Figure S9.** (a, b) SEM images of mesoporous TiO<sub>2</sub> nanosheets (A-MSC-0.03, HF: 0.1 M, 180°C).

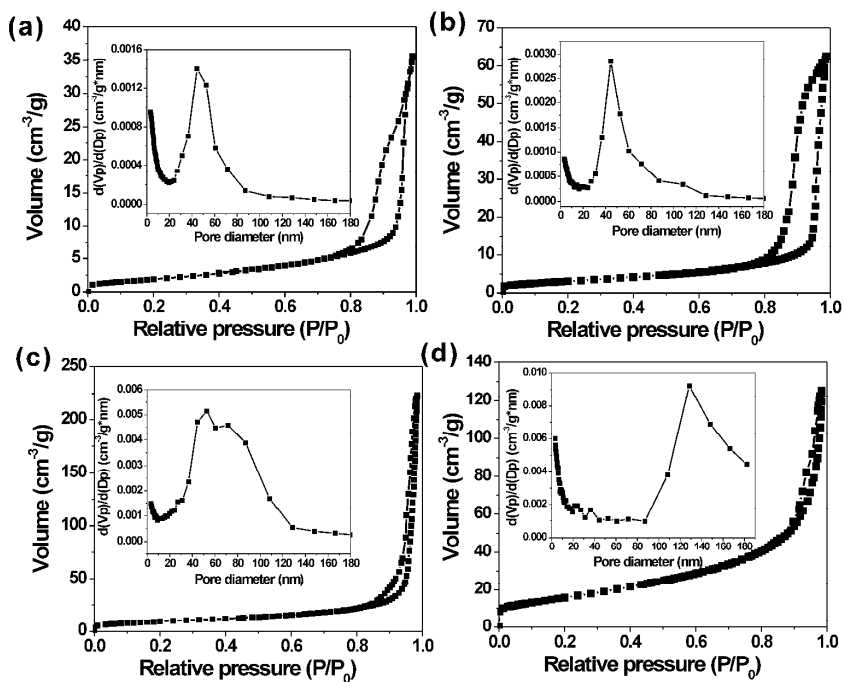


**Figure S10.** N<sub>2</sub> adsorption–desorption isotherms of (a) R-MSC-0.03, (b) R+A-MSC-0.03 (HF: 0.05 M), (c) R-MSC-15 and (d) P25. The corresponding pore size distributions derived from adsorption isotherm are shown in the insets.

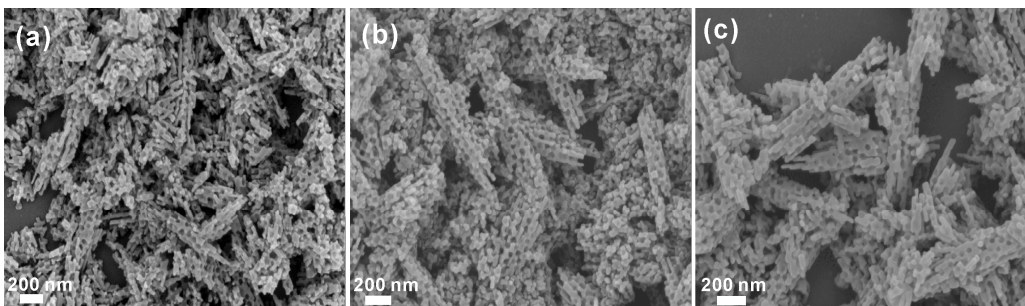


**Figure S11.** SEM images of R-MSC-15 prepared at different temperatures: (a) 150°C, (b) 180°C, (c) 200°C. The sizes of the mesoporous single crystals didn't change with the growth temperature.

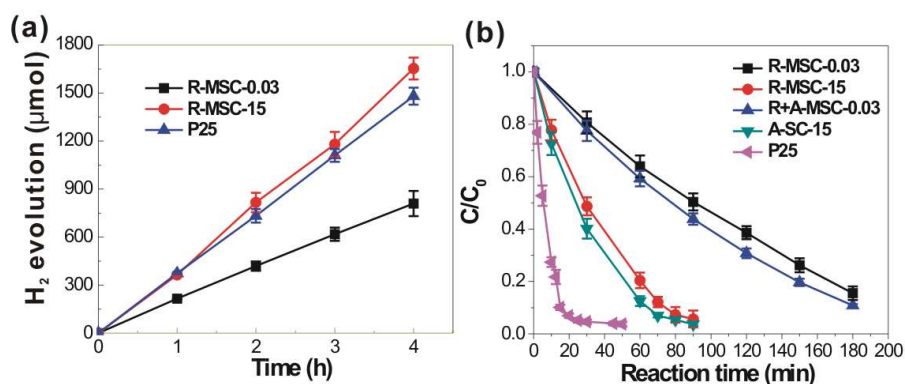


**Figure S12.** (a) Hydrogen evolution curves of R-MSC-0.03, R-MSC-15 and P25. (b) Methyl orange (MO) degradation versus irradiation time in the presence of R-MSC-0.03, R-MSC-15, R+A-MSC-0.03 (HF: 0.05 M), A-SC-15 (HF: 0.05 M) and P25, respectively. Error bars represent the standard deviations of the measured data points based on three samples.

The mesoporous TiO<sub>2</sub> single crystals exhibit lower catalytic ability for the degradation of MO than that of P25. It indicates that the surface area is the dominating factor to influence the photooxidative activity of mesoporous TiO<sub>2</sub> single crystals for the degradation of MO when compared with P25.

**Table S1.** H<sub>2</sub> evolution rate of the TiO<sub>2</sub> products and P25<sup>a</sup>

Sample	H <sub>2</sub> evolution rate ( $\mu\text{mol h}^{-1} \text{g}^{-1}$ )	Sample	H <sub>2</sub> evolution rate ( $\mu\text{mol h}^{-1} \text{g}^{-1}$ )
R-SC	4,011 $\pm$ 243	A-SC	879 $\pm$ 47
R-MS-0.03	6,939 $\pm$ 405	A-MS-0.3	4,158 $\pm$ 282
R-MS-0.3	9,005 $\pm$ 431	P25	12,337 $\pm$ 444
R-MS-15	13,153 $\pm$ 502		

<sup>a</sup> The error estimate was based on three as-prepared samples